The photoionization of methoxymethanol: Fingerprinting a reactive C_2 oxygenate in a complex reactive mixture

Niko A. Hansen,[1] Trevor D. Price,[1] Leah R. Filardi,[1] Sadi M. Gurses,[1] Wenqi Zhou,[1] Nils Hansen,[2] David L. Osborn,[1,2] Judit Zádor,[2] Coleman X. Kronawitter[1,*]

[1]Department of Chemical Engineering, University of California, Davis, California 95616, USA

[2]Combustion Research Facility, Sandia National Laboratories, Livermore, California 94551, USA

Abstract

Methoxymethanol (CH_3OCH_2OH) is a reactive C_2 ether-alcohol that is formed by coupling events in both heterogeneous and homogeneous systems. It is found in complex reactive environments – for example those associated with catalytic reactors, combustion systems, and liquid-phase mixtures of oxygenates. Using tunable synchrotron-generated vacuum-ultraviolet (VUV) photons between 10.0-11.5 eV, we report on the photoionization spectroscopy of methoxymethanol. We determine that the lowest-energy photoionization process is the dissociative ionization of methoxymethanol via H-atom loss to produce $[C_2H_5O_2]^+$, a fragment cation with a mass-to-charge ratio (m/z) = 61.029. We measure the appearance energy of this fragment ion to be 10.24 ± 0.05 eV. The parent cation is not detected in the energy range examined. To elucidate the origin of the m/z = 61.029 ($C_2H_5O_2$) fragment, we used automated electronic structure calculations to identify key stationary points on the cation potential energy surface (PES) and compute conformer-specific microcanonical rate coefficients for the important unimolecular processes. The calculated H-atom dissociation pathway results in a $[C_2H_5O_2]^+$ fragment appearance at 10.21 eV, in excellent agreement with experimental results.

Introduction

Knowledge of molecule-specific spectroscopic fingerprints and physico-chemical characteristics is a prerequisite for identification of key reactive intermediates comprising complex reaction networks in chemical transformations, such as in combustion, catalysis, and plasma-driven reactions. Ongoing research efforts to unravel such complex chemical mechanisms are motivated by grand challenges associated with increasing the efficiency and selectivity of chemical syntheses and reducing the carbon footprint of chemical manufacturing and energy production. The identification of ephemeral intermediate species involved in these reaction networks can be especially challenging due to their transient nature, low concentrations, and the presence of many other species.

One such elusive intermediate is methoxymethanol (CH_3OCH_2OH, also referred to as *hemimethylal*, *hemiformal*, *methoxylated methylene glycol,* and *methoxy monoglycol*). This molecule forms through oxygenate coupling events in heterogeneous[1–3] and homogeneous[4–7] systems. In general, methoxymethanol forms by interactions of formaldehyde with methanol: it is the hemiacetal formed by methanol addition to formaldehyde, which occurs in the absence of a catalyst:[8]

$$CH_3OH + HCHO \rightleftharpoons CH_3OCH_2OH$$

However, in systems containing formaldehyde, methanol, *and water*, the chemical environment is more complex. In these systems, which are ubiquitous in chemistry laboratories because methanol is a common stabilizer added to control formaldehyde oligomerization, methoxymethanol exists within an equilibrated mixture of myriad oxygenates. These species include products of formaldehyde hydration and oligomerization such methylene glycol and its homologues ($HO(CH_2O)_nH$), as well as products of methoxylation – methoxymethanol and larger poly(oxymethylene) hemiformals, ($CH_3(OCH_2)_nOH;\ n \geq 2$).[9] Methoxymethanol can also self-react to form higher hemiformals, releasing methanol with each addition.[9,10]

Methoxymethanol has been identified in the context of catalysis, combustion science, and astrochemistry.[1,3,11-13,18,19-23] In heterogeneous catalysis, it is a reactive intermediate during methanol oxidation over various catalysts[1,3,11–13] where it forms through reactions between formaldehyde and methanol or surface methoxide.[14] Its relevance to applications in heterogeneous catalysis is especially notable because in these systems, methoxymethanol is an intermediate in pathways to value-added chemicals: it can be dehydrogenated[11,15] or transfer a hydrogen atom to formaldehyde[16] to form methyl formate (CH_3OCHO), and in the presence of catalytic acid sites, condense with methanol to form dimethoxymethane ($CH_3OCH_2OCH_3$).[17] Reactions involving methoxymethanol must also be considered for understanding the reaction networks of combustion systems.[18] For example, theoretical work has shown that methoxymethanol might be formed in plasma-assisted combustion through O(^{1}D) insertion into dimethyl ether.[18] Methoxymethanol has also been detected in star-forming regions of interstellar space.[19] Further studies investigated possible formation pathways and detected methoxymethanol among the products resulting from exposure of methanol ice to ionizing radiation, where gas-phase recombination events involving sublimed species yield an array of higher mass organic molecules.[20–23]

In previous reports, methoxymethanol has been identified or characterized using infrared (vibrational),[3,20] millimeter wave (rotational)[24] spectroscopy, and mass

spectrometry with fixed or tunable ionization.[1,2,20–23,25] It is inherently challenging to use vibrational spectroscopies to identify single components in mixtures because of spectral overlaps. The spectral features of methoxymethanol are known to overlap with those of formaldehyde, methanol, and water.[4] Rotational spectroscopy, although the most accurate way to determine structural information of molecules in the gas-phase, is not a highly sensitive technique and therefore is a challenging method for reaction network analysis. Instead, mass spectrometry is inherently well-suited to interrogate the speciation of complex reactive environments.[26] The previously reported mass spectral detections of methoxymethanol in the literature suggest that the indicator for methoxymethanol is a dominant peak at mass-to-charge ratio (m/z) 61 with little to no signal of the expected parent cation at m/z 62.[1,2,20–23,25] Our previous work using electron ionization mass spectrometry with tunable energies to identify and study methoxymethanol produced in catalytic systems also used this indicator.[11–13]

Motivated by the unique capabilities of near-threshold photoionization mass spectrometry to structurally identify key intermediates in complex reactive mixtures,[26–28] we report herein an experimental study of the photoionization of methoxymethanol using synchrotron VUV radiation. Photoionization spectra — ion yield as a function of incident photon energy — provide important fingerprints of reactive molecules via the observed ionization energy, the photoionization spectrum shape that is governed by Franck-Condon factors, and the onset at higher excitation energy of cation fragmentation to specific fragment ions.[26,29] Photoionization is a more powerful approach compared to low-energy-resolution electron ionization because its higher energy resolution provides better spectral fingerprints to identify isomers and improved control of undesired ionization and fragmentation.[26] We use heterogeneous catalytic methanol oxidation as a tool to generate a steady state concentration of gas-phase methoxymethanol to facilitate the measurement of its photoionization spectrum and enable its future identification in other complex systems. We interpret the experimentally obtained photoionization mass spectrometry results using automated first-principles calculations for the exploration of the neutral and cationic potential energy surfaces to capture the unimolecular kinetics of the methoxymethanol cation.

Experimental and Theoretical Methods

Experimental Methods

To acquire the photoionization mass spectra of methoxymethanol, we combined a catalytic flow reactor with an orthogonal extraction, reflectron time-of-flight (TOF) molecular-beam mass spectrometer (MBMS) with a mass resolution (m/Δm) of ~3000 and a sensitivity limit of ~1 ppm. The instrument has been described previously,[26,28,30,31] and only a short summary is provided here. The apparatus consists of a reaction chamber that is connected via a differentially pumped vacuum system to the ionization chamber of the mass spectrometer. Reaction gases are sampled from the reaction chamber by a conical quartz probe with a ~50 μm orifice diameter at the tip, forming a molecular beam that passes through two pumping stages via an intermediate conical nickel skimmer and into the ionization chamber. This molecular beam expands upon rapid pressure reduction,

effectively freezing the gas composition and preserving unstable species by eliminating analyte-analyte collisions.

We ionize the sampled gases using tunable synchrotron VUV light from the Chemical Dynamics Beamline 9.0.2 of the Advanced Light Source at Lawrence Berkeley National Laboratory. The synchrotron radiation is tunable in the range of 7.5-24 eV with a maximum photon flux of 10^{13} photons/s available for photoionization of analyte gases. Subsequent photo-ions are accelerated through a custom-built reflectron (Kaesdorf) time-of-flight analyzer to a microchannel plate detector. Ion counts are recorded as a function of flight time in 0.2 ns bin widths over 2^{23}-2^{24} sweeps of a multichannel scaler. The collected spectra are calibrated to m/z values according to the flight times of $[H_2O]^+$ at m/z = 18.011, $[CH_3O]^+$ (fragment ion of CH_4O) at m/z = 31.018, $[CH_4O]^+$ at m/z = 32.026, $[CO_2]^+$ at m/z = 43.990, and the three primary isotopes of $[Xe]^+$ (^{129}Xe, ^{131}Xe, ^{132}Xe) at m/z = 128.905, 130.905, and 131.904, respectively. All mass calibration spectra are collected at 14.35 eV.

The catalytic flow reactor consisted of a quartz tube (ID ~16 mm) enclosed within a proportional-integral-derivative (PID) controlled, electrically heated furnace for precise temperature control. Both the oven and reactor were surrounded by a stainless-steel chamber. About 250 mg of catalytic Pd/MgO (1 wt%) were loaded into a small quartz boat and positioned in the quartz tube to within ~1 cm of the MBMS sampling cone. Pd/MgO (1 wt%) was prepared via an adapted wet impregnation procedure described previously.[32] Briefly, 1 g of MgO powder (100 nm, U.S. Research Nanomaterials) was suspended in 19 mL of deionized water and stirred at 50°C for 10 minutes to produce an MgO slurry. A Pd precursor solution was prepared by dissolving 16.8 mg of $PdCl_2$ in 1 mL of 0.1 M HCl. The resultant solution was injected into the MgO slurry and stirred at 50°C for 5 h. The ensuing paste was dried in an oven overnight at 80°C in air. Prior to use, the catalyst powder was calcined at 700°C for 6 h under 20% O_2 flow (balance N_2). The resulting powder was pressed into dense pellets and broken up into small, roughly 0.5 cm x 0.5 cm, fragments.

For the reactive gas mixture, methanol vapor was introduced to the reactor by bubbling Ar (Matheson >99.9999%) through liquid methanol maintained at 25°C in an isothermal water bath. The vapor pressure of methanol at 25°C is 94 Torr, and the total pressure at the outlet of the bubbler was maintained at 200 Torr, yielding a methanol composition of 47% at the outlet of the bubbler. The bubbler outlet stream was mixed with O_2 (Matheson >99.994%) and diluted with Ar to yield flows of 10 sccm, 8.0 sccm, and 16 sccm for methanol bubbler output, O_2, and Ar, respectively. An additional diluent line of Xe (Matheson >99.999%) was included with flow at 1 sccm to monitor the consistency of total ion counts and calibrate mass spectra. Source gases were controlled using calibrated mass flow controllers and exhaust gases were continuously pumped out to sustain constant chamber pressure at 20 Torr. The catalyst bed was maintained at an isothermal 353 K during reaction.

Theoretical Methods

We used the KinBot[33,34] kinetics workflow code to explore and characterize the important stationary points of the neutral and cationic surfaces of methoxymethanol through automated electronic structure calculations. We carried out the conformer search on the neutral PES using Kinbot at the B3LYP/6-31G(d) level of theory on a 120-degree grid for the C-O-C-O and O-C-O-H conformer-generating torsions, and refined the rovibrational properties at the ωB97X-D/6-311++G(d,p) level. The typical uncertainty of the coupled cluster calculations is about 0.04 - 0.09 eV. Our level of density functional theory (DFT) is uncertain by about 0.09 - 0.17 eV. However, when ionization energies and relative conformer energies are calculated, we expect a slightly better accuracy due to error cancellation. Further assessment of the true errors in all calculated values is beyond the scope of this work. For select properties we also computed CBS-QB3[35] energies, which are shown in the Supplementary Material. To account for anharmonicities in the sum and density of states, we used two approaches. In one, we used a separable one-dimensional hindered rotor (HR) approximations for all rotatable dihedrals, projecting out the components of the Hessian corresponding to these motions. In the other, we treated the various conformers separately as a rigid-rotor-harmonic-oscillator (RRHO). The two approaches, in principle, should give the same answer at low energies, however, as we will show, the latter approach is preferred for our system because of the coupled motion of the rotors. For reactions with a barrier, it is important to consider quantum mechanical tunneling that can result in the appearance of products at energies below the barrier height. We include tunneling in our calculations by approximating the barrier as a one-dimensional Eckart barrier. The DFT values were obtained using Gaussian 16,[36] while the coupled-cluster energies were calculated with Molpro 2022.[37] The molecular properties required for the Rice-Ramsperger-Kassel-Marcus (RRKM) calculations were automatically assembled by KinBot into an input file, and the microcanonical rate coefficients were evaluated with the Master Equation System Solver (MESS) code.[38]

Results and Discussion

Experimental Results

Representative mass spectra for our methanol partial oxidation reaction system are shown in Fig. 1 for photon energies of 10.0 eV, 11.5 eV, and 14.35 eV with peaks assigned to the observed neutral reactant and product molecules. The most prominent peaks appear at m/z = 18.011 (H_2O), 31.990 (O_2), 32.026 (CH_4O), 44.990 (CO_2), 44.993 ($^{13}CO_2$), 45.034 (C_2H_5O), and 60.021 ($C_2H_4O_2$). Peaks near m/z 61 and 62 can be ascribed to the ^{13}C, ^{17}O, ^{18}O, and ^{2}H isotopologues of $C_2H_4O_2$ and/or $C_2H_5O_2$ and $C_2H_6O_2$. A mass resolution of more than 8000 is necessary to separate the individual components to the respective m/z 61 and 62 peaks; therefore, we treat each as a single peak and refer to them as m/z 61 and 62.

While the lower mass peaks are related either to the reactants (oxygen and methanol) and products of complete oxidation (water and CO_2), we focus on the peaks located at m/z = 45.034 $[C_2H_5O]^+$, 61, and 62, because they potentially originate from the parent cation of methoxymethanol $[C_2H_6O_2]^+$ and its fragment cations.[11,20,22,39] The peak at m/z = 60.021 is attributed to $C_2H_4O_2$; however, given its strong signal compared to m/z 61 and 62 (see Fig. 1), it is important to first determine its identity and origin.

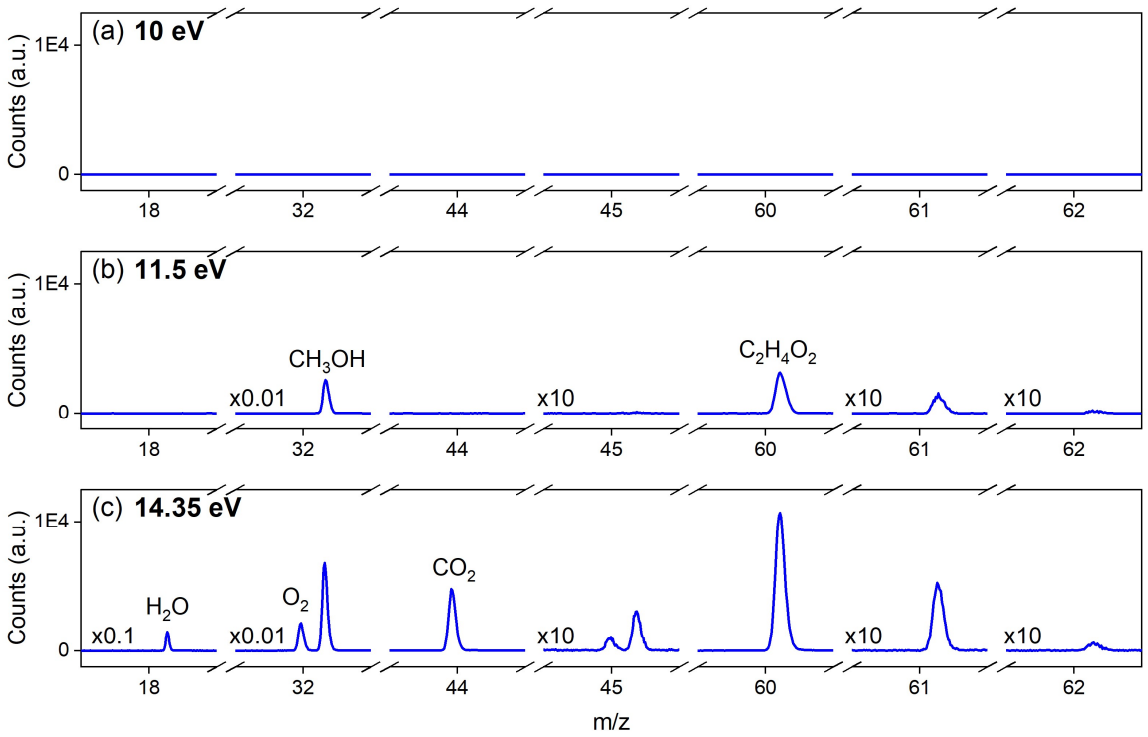

Fig. 1: Photoionization mass spectra taken at (a) 10.0 eV; (b) 11.5 eV; and (c) 14.35 eV. Peaks are labeled with neutral sum formulae. Data were collected during partial methanol oxidation over Pd/MgO.

To correctly identify the species that yields a cation at m/z = 60.021, we recorded a photoionization spectrum from 10.0-11.5 eV. Fig. 2a shows our observed photoionization spectrum compared with a normalized reference spectrum[31] of an authentic methyl formate sample (shown by short-dashed line), which is in excellent agreement. As mentioned in the Introduction, methoxymethanol can be an intermediate in the generation of methyl formate by methanol oxidation; in our previous work with Pd-based catalysts,[11,13] we observed that the two species are produced concurrently in all experimental conditions examined. Therefore, we assign the peak at m/z = 60.021 in these photoionization experiments to methyl formate. Having identified m/z = 60.021 as methyl formate, it is important to note that its naturally abundant isotopologues (containing ^{13}C, ^{17}O, ^{18}O, and ^{2}H) coincide with the m/z 61 and 62 signals we may expect from the targeted methoxymethanol.

To unambiguously identify the targeted fingerprint for methoxymethanol, we recorded a photoionization spectrum from 10.0-11.5 eV with particular focus on signal at m/z = 62, 61, and 45 as they are potentially associated with methoxymethanol. The peak at m/z = 62.037 matches the exact mass expected for $[C_2H_6O_2]^+$, which would be consistent with the parent cation of methoxymethanol. The calculated adiabatic ionization energy (AIE) of methoxymethanol was previously determined by Zhu et al. as 10.12 eV at the CCSD(T)/CBS//B3LYP/aug-cc-pVTZ level of theory,[22] and as 10.05 eV by Moshammer et al. at the QCISD(T)/aug-cc-pVTZ + MP2/CBS − MP2/aug-cc-pVTZ level of theory.[28]

Fig. 2a shows the photoionization spectra for m/z 62 together with the sampled and reference photoionization spectra[31] of methyl formate at m/z = 60.021. The qualitative agreement between m/z 62 and the methyl formate signal at m/z 60 suggests that the signal at m/z 62 may be attributed wholly to isotopologues of methyl formate; however, Fig. S3b shows that significant residual m/z 62 signal remains after subtracting the signal of the ^{13}C, ^{17}O, ^{18}O, and ^{2}H isotopologues of methyl formate The observed residual m/z 62 signal can be explained by the ^{13}C, ^{17}O, ^{18}O, and ^{2}H isotopologues of $C_2H_5O_2$ (see Fig. S3a) and phenomena associated with instrument sampling and detection (see Supplemental Material for further discussion). Therefore, we report no detectable signal for the methoxymethanol parent cation below 11.5 eV and we can deduce that the parent ion at m/z = 62.037 is not stable. When the m/z 62 parent cation signal has been reported in prior catalysis studies[11,20,22,39] its intensity is consistently very low, and its presence can likely be attributed to the natural abundance of heavier isotopologues of the m/z 61 fragment ion and methyl formate, which, as noted above, is often produced concurrently in catalytic systems. With no detectable parent cation signal, we shift our focus to the signals at m/z 61 and 45 as potential fingerprints of methoxymethanol.

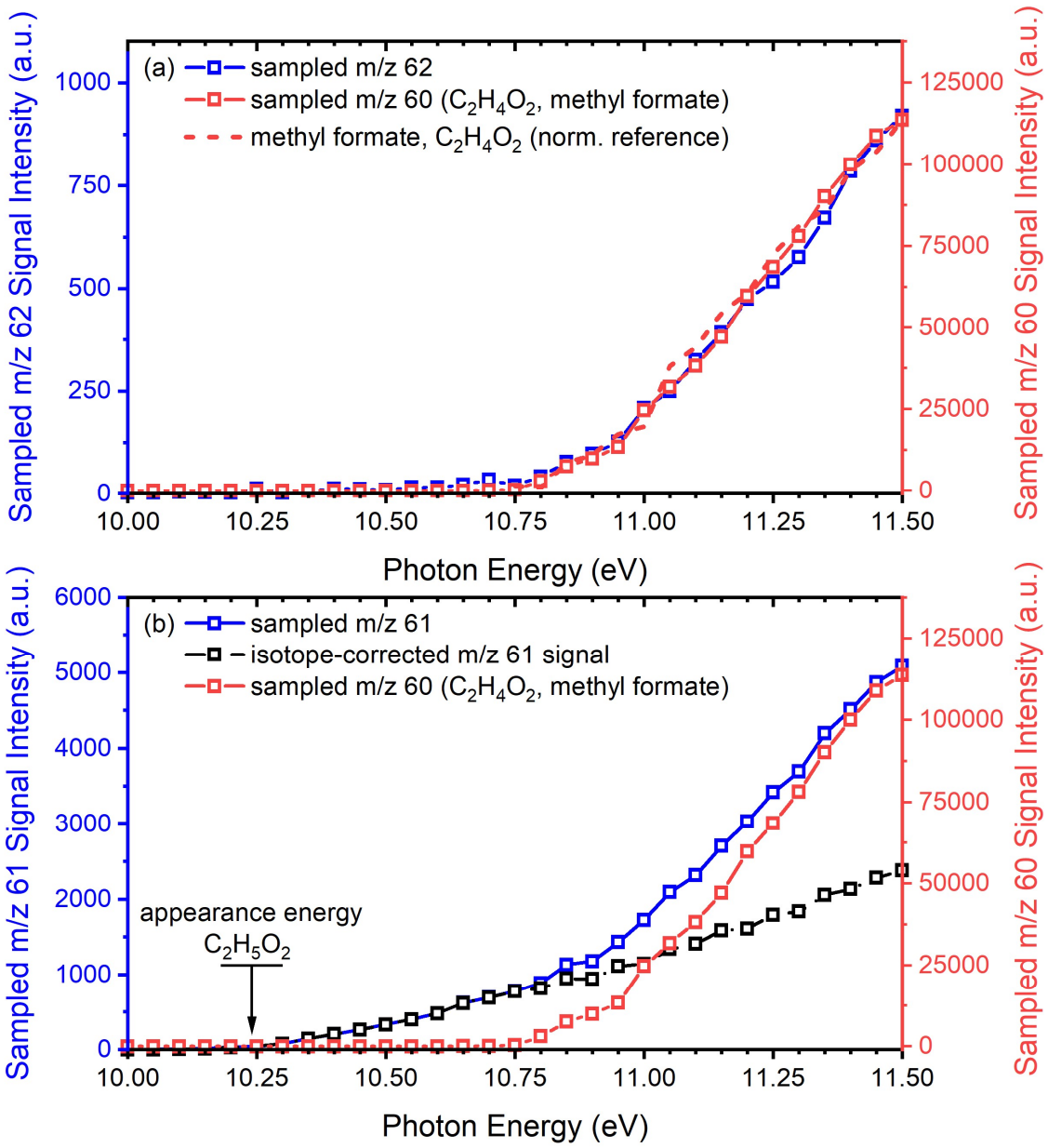

Fig. 2: Qualitative comparison of the sampled photoionization spectra from 10.0-11.5 eV of the reactor effluent at (a) m/z 62 and m/z 60 vs the reference spectrum of an authentic methyl formate sample;[31] (b) m/z 61 vs isotope-corrected m/z 61 according to natural abundance of methyl formate ^{13}C, ^{17}O, ^{18}O, and ^{2}H isotopologues vs sampled methyl formate.

Fig. 2b shows the sampled photoionization spectra for m/z 61. We determined the onset energy to be 10.24 ± 0.05 eV (see Fig. S1a). In a chemical system composed of C, H, and O atoms, strong signals at odd m/z ratios, interpreted as parent ions, must represent neutral free radicals; however, it is unlikely that the $[C_2H_5O_2]^+$ signal represents a neutral free radical for the following reasons. First, $C_2H_5O_2$ radical isomers are expected to have lower ionization energies than 10.24 eV. As an example, the ethyl peroxy radical

(CH_3CH_2OO) has a calculated AIE = 9.48 eV and does not have a stable parent cation.[40] To consider the ionization of free radicals, we calculated IEs for the three radicals possible via H loss from methoxymethanol (forming singlet and triplet cations), namely CH_2OCH_2OH, CH_3OCHOH, and CH_3OCH_2O. Of these, only ionization to the triplet state cation of the oxy-radical CH_3OCH_2O lies above 10 eV. This neutral oxy-radical, isoelectronic with the OH and CH_3O radicals, would be highly reactive, and hence we expect its steady-state concentration would be much smaller than the concentration of closed-shell methoxymethanol. Therefore, we now explore the possibility that m/z = 61.029 may arise from methoxymethanol's dissociative ionization via H-atom loss on the cation surface. The lack of parent ion signal is common for similar oxygenates,[30,40,41] and the loss of an H-atom upon ionization is typical for alcohols.

As seen in Fig. 2b, no methyl formate signal at m/z 60 is observed below 10.75 eV; thus, isotopic contributions from methyl formate to signal at m/z 61 can be ruled out in this energy range. Therefore, the signal at m/z 61 below 10.75 eV can be confidently assigned to the $C_2H_5O_2$ fragment caused by methoxymethanol dissociative ionization processes. The exact mass of $[C_2H_5O_2]^+$ is 61.029 amu, which agrees well with our measured mass peak of 61.032, supporting the assignment to this chemical composition. After correcting the signal above 10.75 eV for contributions from the ^{13}C, ^{17}O, ^{18}O, and ^{2}H isotopologues of methyl formate, the signal shown by the black squares and line in Fig. 2b remains. The persisting signal is the characteristic photoionization spectrum of the $[C_2H_5O_2]^+$ fragment cation from dissociative ionization of methoxymethanol via H-atom loss.

In earlier work, dimethoxymethane ($CH_3OCH_2OCH_3$) was identified as another concurrently produced species during methanol oxidation over Pd-based catalysts. Ionization of dimethoxymethane (parent ion $[C_3H_8O_2]^+$ at m/z 76) yields two major fragments: $[C_3H_7O_2]^+$ at m/z = 75.045 and $[C_2H_5O]^+$ at m/z = 45.034, with no parent ion observation.[30] Our measured mass peaks of 75.050 amu and 45.037 amu support the assignment to these chemical compositions. Fig. S2a shows our sampled photoionization spectrum for m/z = 75.050 $[C_3H_7O_3]^+$ compared with a reference spectrum[30] of the m/z 75 fragment of an authentic dimethoxymethane sample. The excellent qualitative agreement between the two spectra up to 10.8 eV leads us to attribute the $[C_3H_7O_2]^+$ ion to dimethoxymethane. Beyond 10.8 eV, significant deviation from the reference spectrum suggests that multiple effluent species or fragments of higher mass molecules contribute to our signal at m/z = 75.050.

Fig. S2b shows our sampled photoionization spectrum for m/z = 45.037 $[C_2H_5O]^+$ compared with a reference spectrum[30] of the m/z 45 fragment of an authentic dimethoxymethane sample. The relative intensity of our sampled m/z 45 spectrum is larger than that of the reference spectrum, which implies that a large fraction of the signal sampled at m/z 45 cannot be attributed to the fragment of concurrently produced dimethoxymethane. This observation, as well as the previous observation of m/z 45 from gas chromatography/mass spectrometry (GC/MS) studies on methoxymethanol,[20] motivated our consideration of $[C_2H_5O]^+$ as a possible fragment of methoxymethanol. Analysis in Fig. S1b indicates an onset energy of 10.78 eV ± 0.05 eV. We note, however, that the OH-loss channel for alcohols is typically very minimal, appearing at higher photon

energies, if at all.[29] This, along with the observations made in the introduction – that methoxymethanol almost always appears in complex mixtures of oxygenates[9] – suggests that if m/z 45 is part of the fragmentation pattern of methoxymethanol, it is not a reliable fingerprint of its presence.

Finally, we considered two additional potential fingerprint fragment ions of methoxymethanol: $[C_2H_4O]^+$ at m/z 44 via the H_2O-loss channel and $[CH_3O]^+$ at m/z 31 via the CH_3O-loss channel. The signal from $[C_2H_4O]^+$ at m/z = 44.026 does not include contributions from carbon dioxide $[CO_2]^+$, (m/z = 43.990) for two reasons: our photon energies are well below the 13.777 eV ionization energy of CO_2 and the mass resolution of the instrument is sufficient to separate these signals. Neither methyl formate nor dimethoxymethane produce a fragment cation at m/z 44 in our selected energy range.[30,31] As shown in Fig. 1, no peak was observed at m/z 44 at 10.0 or 11.5 eV; therefore, H_2O-loss of methoxymethanol does not occur within our sampled energy range. The signal from $[CH_3O]^+$ at m/z 31, which has also previously been observed,[20] cannot be studied here because of the inherent conflict of the H-loss fragments and ^{13}C isotopologues of methanol and formaldehyde, which exist in abundance in our system and which exist in alongside methoxymethanol in equilibrated systems where it is found.[8]

Based on our experimental analyses, we determine that the lowest-energy ionization event in the photoionization process of methoxymethanol is dissociative ionization via H-atom loss to produce the fragment cation $[C_2H_5O_2]^+$, at m/z = 61.029. Our conclusion that ionized methoxymethanol is observed at its primary fragment cation at m/z 61 is consistent with all previously published mass spectra recorded at fixed energies.[1,2,11,20–22,25,39] We determine the appearance energy of this fragment cation as 10.24 ± 0.05, which can be used to identify methoxymethanol within reactive mixtures. Below, we present a detailed theoretical investigation of the neutral and cation potential energy surfaces to describe the mechanism and kinetics of dissociative ionization of methoxymethanol and thus identify the origin of the m/z 61 signal.

Electronic Structure and Cation Unimolecular Dissociation Kinetics Calculations

Three neutral conformers (Fig. 3) of methoxymethanol have previously been identified in a computational study by Hays and Widicus-Weaver employing the MP2/aug-cc-pVTZ method for geometry optimization followed by single point energies at the CCSD(T)/aug-cc-pVTZ level of theory.[42] We also found three conformer pairs consisting of mirror images. The relative energies of the pairs are 0.00, 0.09, and 0.10 eV (including zero-point energy (ZPE)) at the ωB97X-D/6-311++G(d,p) as shown in Fig. 3. The relative energy of 0.09 eV is equivalent to less than 2% population at 300 K, thus only the lowest energy conformer of the neutral is considered in the following. A temperature of 300 K is considered as it is the temperature of the sampled molecular beam at the point of ionization within the MBMS instrument.[26,43] Note that additional calculations at the CBS-QB3 level yielded essentially the same results (See Fig. S4). Furthermore, prior work has determined that the barriers for interconversion among the neutral conformers are small enough (< 0.2 eV) to assume an equilibrium distribution of the three conformers even at 300 K.[24]

We identified four cation conformers, with relative energies of 0.000, 0.184, 0.230 and 0.234 eV at the ωB97X-D/6-311++G(d,p) level also shown in Fig. 3. Note that in prior calculations, Zhu et al. found only two unique methoxymethanol cation conformers — *gauche*-methoxymethanol and *eclipsed*-methoxymethanol.[22] In agreement with the previous work, our calculations show that the lowest energy conformer is the gauche structure; however, this is not the species that is obtained via geometry optimization when an electron is removed from the lowest energy neutral conformer. Instead, at the ωB97X-D/6-311++G(d,p) level the cation converges to the eclipsed structure. This result contrasts with our CBS-QB3 calculations, where removal of an electron from the lowest-energy neutral conformer optimizes to the gauche cation conformer. A more detailed look revealed that the reason for this discrepancy is that the neutral geometry is close to a conformational saddle on the cationic surface, and minor differences in the details of the optimization and in the level of theory can drive the optimization towards different conformers. The calculated AIE at the CCSD(T)-F12a/cc-pVTZ-F12//ωB97X-D/6-311++G(d,p) level is 10.00 eV, which is in good agreement with the value of Moshammer et al. (10.05 eV),[28] and in a reasonable agreement with that of Zhu et al. (10.12 eV).[22]

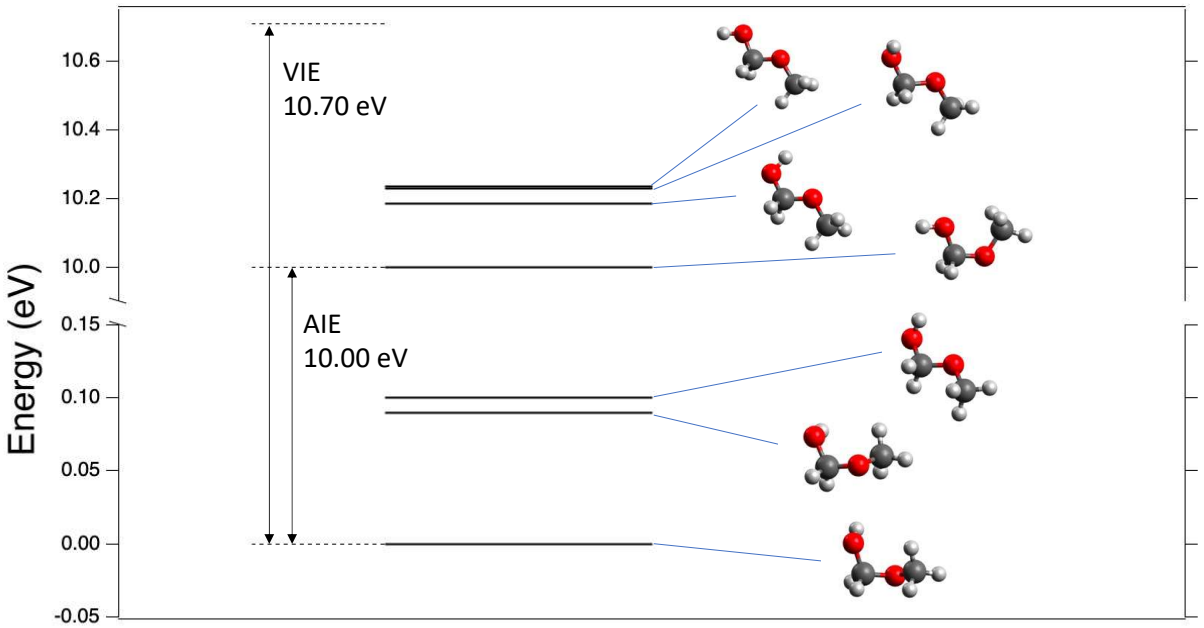

Fig. 3: Energy diagram of methoxymethanol ionization. The relative energies of the conformers are calculated at the ωB97X-D/6-311++G(d,p) level, while the AIE is calculated at the CCSD(T)-F12a/cc-pVTZ-F12//ωB97X-D/6-311++G(d,p) level, in both cases including ZPE corrections. The vertical ionization energy is calculated without ZPE correction.

However, irrespective of the conformer to which the direct ionization leads, the neutral and the cation structures differ at least in their C–O–C–O backbone dihedral angles significantly enough to expect negligible Franck-Condon overlap at the AIE.

Specifically, the C–O–C–O dihedral angle is 68.3° in the neutral structure, while in the lowest energy gauche cation conformer it is 0.0° and in the eclipsed cation conformer reached by optimization from the neutral global minimum geometry it is 166.1°. Thus, despite a calculated AIE of 10.00 eV, no ionization of methoxymethanol is expected at this energy. The vertical ionization energy (VIE) of the system is 10.70 eV (not including ZPE).

We found three feasible reaction channels on the cationic PES shown in Fig. 4. The lowest energy process leads to the loss of an H-atom, while the higher pathways result in loss of a water molecule or an OH-radical. There are five saddle points for H-atom loss that differ only in their torsional conformations. We denote these as TS_{H1} to TS_{H5} in order of increasing saddle point energy and discuss below the impact of these saddle point conformers on the unimolecular kinetics. For simplicity, Fig. 4 plots only the lowest of these saddle points, TS_{H1}. Note the deep postreaction complexes formed in the case of OH and particularly in the case of the H_2O-loss channels. These complexes are held together by strong ion-dipole interactions. In the following we focus on the two lowest energy processes, the H-loss and H_2O-loss, and discard the OH-loss channel, which is above the VIE. Note that another straightforward channel, dissociation along the C–O bond is also possible, yielding the instantaneous products of $[CH_3O]^+ + CH_2OH$ or $CH_3O + [CH_2OH]^+$, each fragment with m/z 31. The CH_3O^+ cation spontaneously rearranges to $[CH_2O]^+$. In the end, both combinations of product pairs lie too high, about 1.4 eV above the methoxymethanol cation, and, therefore, are excluded as well from further considerations.

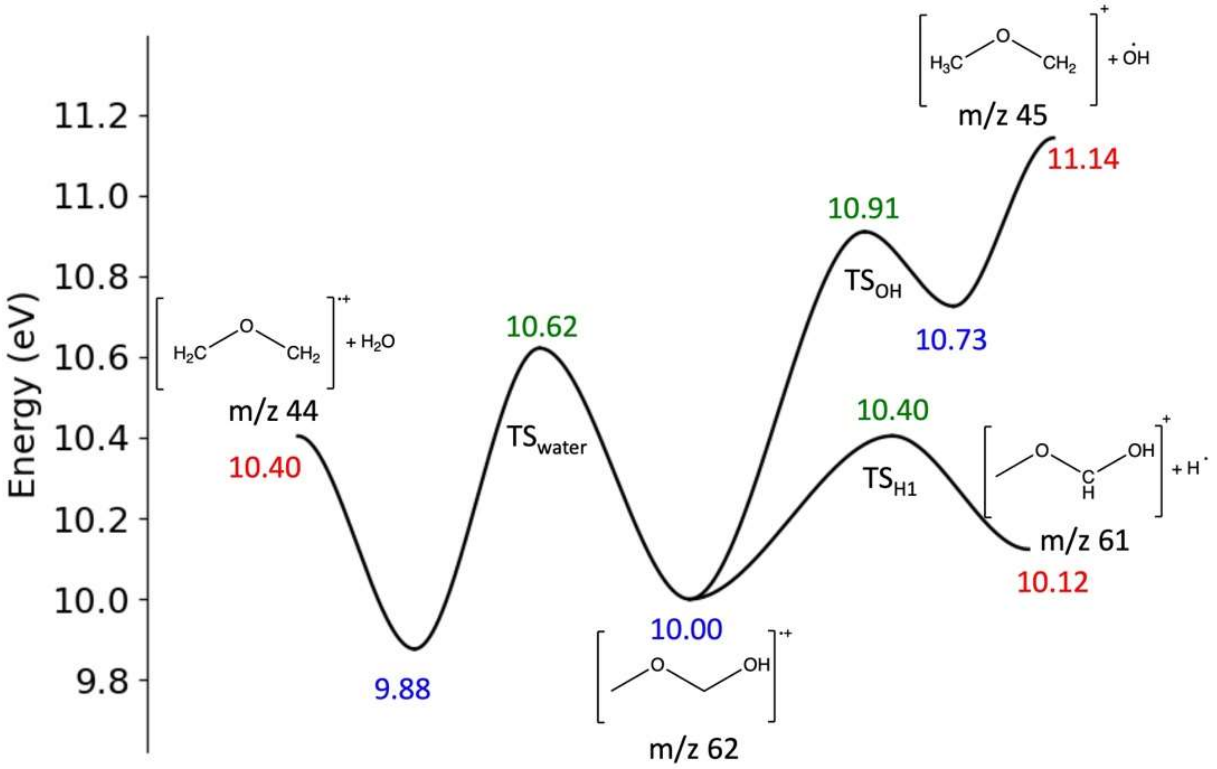

Fig. 4: The cationic reactive PES of $[C_2H_6O_2]^+$. The energies are relative to the lowest energy neutral structure and are calculated at the CCSD(T)-F12a/cc-pVTZ-F12//ωB97X-D/6-311++G(d,p) level, including ZPE correction, and correspond to the lowest energy conformer of the stationary points. Energies are color coded as $[C_2H_6O_2]^+$ minima (blue), 1st order saddle points (green), bimolecular products (red).

We calculated RRKM rate coefficients, $k(E)$, as a function of excitation energy E for unimolecular decomposition via the two lower channels, with results shown in Fig. 5. Unfortunately, when the motion along the dihedral angles of TS_{H1} are projected out from the Hessian, the imaginary frequency—a key parameter in our tunneling model—vanishes: the original 890i cm^{-1} value becomes approx. 100 cm^{-1}, i.e., small, and non-imaginary. This change can happen because of mode mixing that is not well represented by a separable 1-D hindered rotor model. Indeed, the normal mode analysis of the saddle point shows that the motion of the leaving H-atom contributes significantly to many low-frequency normal mode displacement vectors. We address this difficulty in two ways. In one set of calculations, we replace this small real frequency with its complex conjugate and compute the unimolecular rate coefficient for H-loss using the anharmonic state count model for TS_{H1}. In a second set of calculations, we explore the kinetics resolved at the conformational level using a simpler RRHO model for state counting in all vibrational degrees of freedom. Importantly, the RRHO method retains the magnitude of the imaginary frequency at the saddle points.

The orange curve labeled $TS_{H,HR}$ in Fig. 5 plots k(E) for H-atom loss—yielding m/z 61—in the HR model. The $TS_{H,HR}$ curve implicitly includes the energy-weighted contribution of the other H-loss saddle points, with the most important contribution from the lowest energy saddle point, TS_{H1}. The effect of quantum mechanical tunneling can be seen as a finite rate coefficient for $E < E(TS_{H1}) = 10.40$ eV. However, the effect of tunneling is muted by the small magnitude (~100i cm^{-1}) of the imaginary frequency. The saddle point for water loss, TS_{water}, has a much higher imaginary frequency, and as a result a much wider energy range ($E < 10.62$ eV) over which tunneling contributes in Fig. 5. Nevertheless, the $k(E)$ for H_2O-loss is much smaller than for H-loss, and, therefore, our calculations predict that water loss in methoxymethanol photoionization will be unimportant for our experiments where $E < 10.5$ eV.

Focusing again on the H-loss pathways from the methoxymethanol cation, Fig. 6 shows in more detail the barriers for conformational isomerization and H-loss (all first-order saddle points). Of the four cation conformers, the three high-energy conformers (10.18, 10.23, and 10.23 eV in Fig. 6) interconvert rapidly across low barriers, whereas the lowest energy conformer is separated from the others via a relatively high barrier (TS_{conf}) that is only 0.07 eV below the lowest H-loss barrier, TS_{H1}. We use this picture to compare our RRKM rate coefficients calculated in a purely RRHO framework (i.e., no hindered rotors) for three important pathways. These are, in Fig. 5: the conversion of the lowest energy conformer to the others via TS_{conf} (green line), H-loss of the lowest energy conformer via TS_{H1} (blue line), and H-loss from the higher-energy conformer group to products via TS_{H2} (black line). These results imply that for $E < 10.3$ eV, H-loss dominates

over conformational isomerization. However, at $E \geq 10.35$ eV, the four methoxymethanol cation conformers interconvert on the same timescale as H-loss, and hence the distinction between these four conformers becomes less important at these higher energies. The RRHO model (black and blue lines of Fig. 5) predicts a lower onset energy for H-loss than the anharmonic model.

Finally, it is important to compare the uncertainties in the hindered rotor and the RRHO model. The hindered rotor model seems to have difficulty including the very important tunneling effects due to the coupling of the reaction coordinate with the internal rotor motions, while the RRHO model, by construction, carries increasing uncertainties with increasing energies in $k(E)$. To identify fragments, our main focus in this work is to determine onsets, therefore, we believe that the independent RRHO model is more appropriate for the purposes of this study.

Experimentally, a necessary condition for a fragment ion to be detected is that it is formed on a timescale shorter than the time the ion needs to reach the electric field-free region of the instrument, i.e., the time between ionization and the field-free region must be shorter than $1/k(E)$. This characteristic time in our TOF-MS is 13.8 μs for ions near m/z 61, represented as the horizontal dashed line in Fig. 5. Considering the more reliable RRHO model and including a red shift of 0.026 eV to account for the 300 K temperature of the experimental molecular beam, the two relevant rate coefficients cross the 13.8 μs line at 10.21 and 10.22 eV, in excellent agreement with the experimental appearance energy of 10.24 ± 0.05 eV.

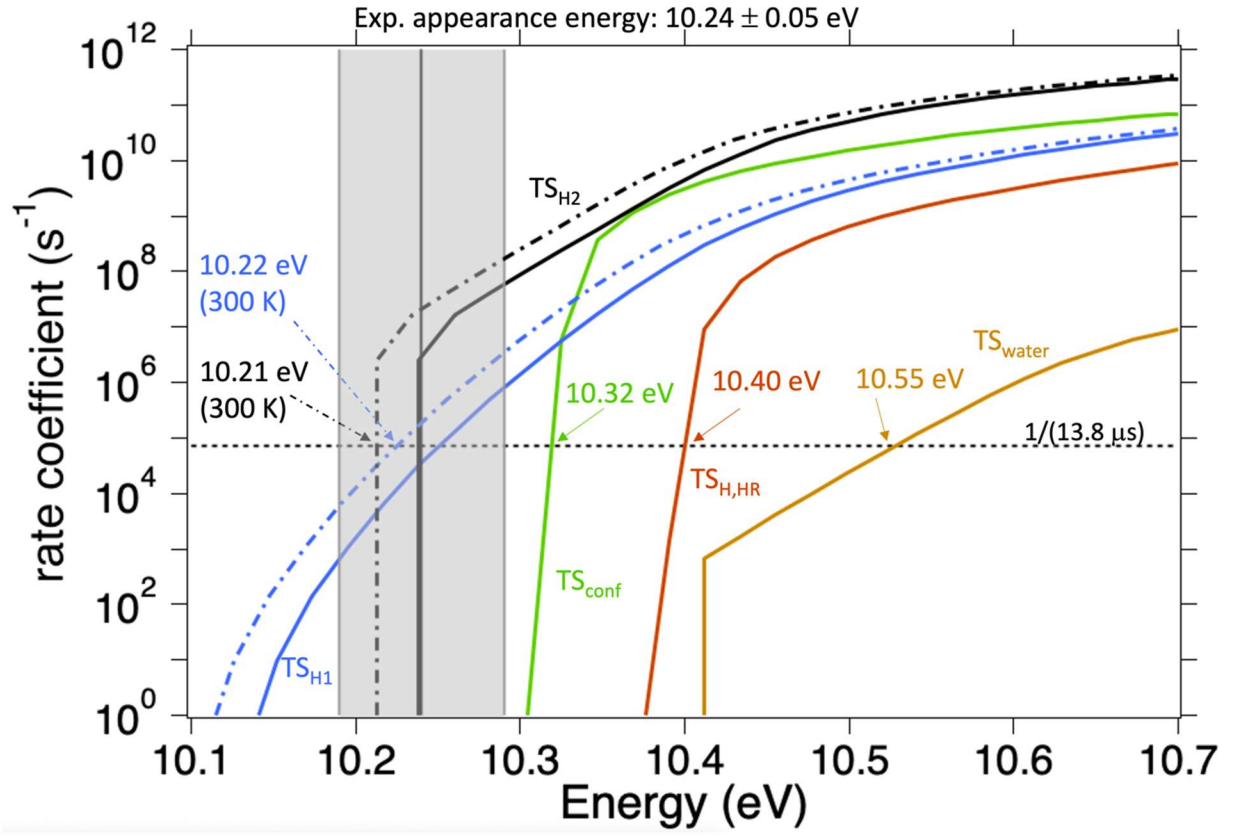

Fig. 5: RRKM rate coefficients in various models for various processes. The TS labels refer to the transition states shown in Figs. 4 and 6. The horizontal dashed line indicates the flight time in the orthogonal extraction region (13.8 μs), and the energies listed near the arrows are the ones at which our models predict the corresponding processes to be than that, i.e., k > 1/(13.8 μs) = 72464 s^{-1}. The experimental appearance energy (dark gray vertical line) and its error bar (gray shaded region) are also shown. The dash-dot lines for TS_{H1} and TS_{H2} are red-shifted by 0.026 eV to account for the temperature (300 K) of the molecular beam in the ionization region. All other solid lines are calculated at 0 K.

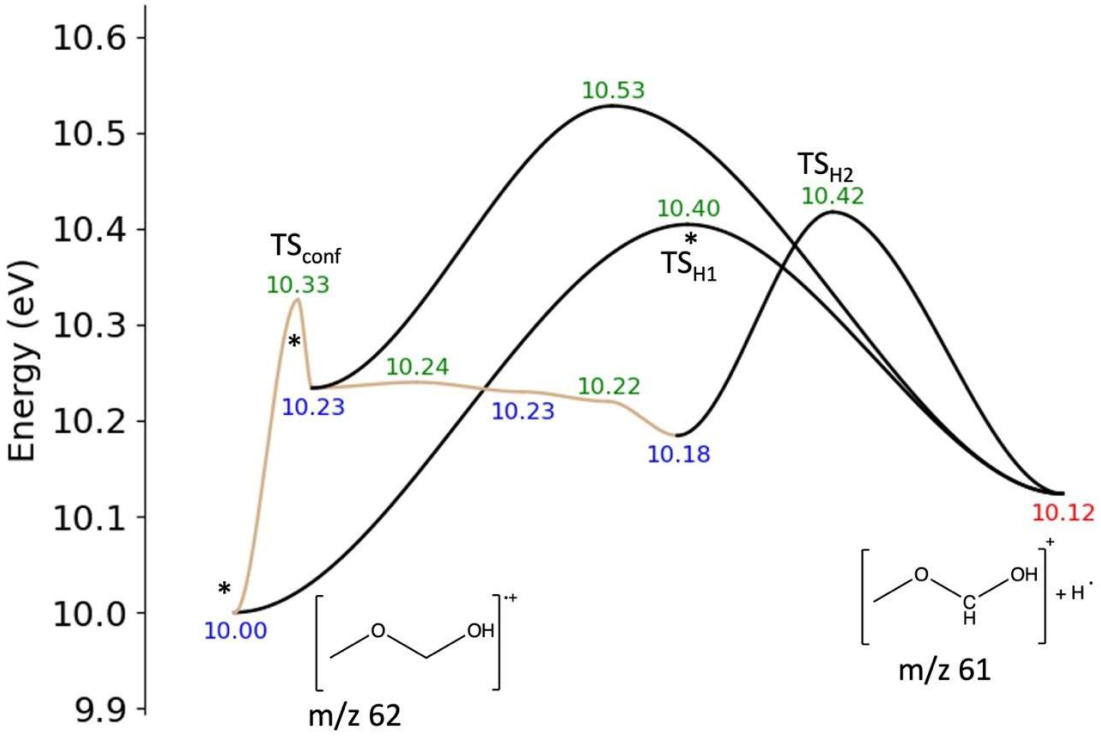

Fig. 6: Important low-energy conformational barriers (tan) and reaction pathways (black) of the methoxymethanol cation in the H-loss channel forming m/z 61. All relative barrier heights are included in green. Relative energies of the m/z 62 conformers are included in blue, with the final dehydrogenated m/z 61 product included in red. The lowest energy conformer of the m/z 62 cation (10.00 eV), the most important reactive pathway (via TS_{H1}), and the bottle-neck conformer pathway (via TS_{conf}) are characterized at the CCSD(T)-F12a/cc-pVTZ-F12//ωB97X-D/6-311++G(d,p) level relative to the lowest energy conformer of the neutral (these are marked with asterisks). The other energies are provided at the ωB97X-D/6-311++G(d,p) level in a relative sense. The conformers of the product and some higher energy conformers of the reaction path are ignored. All energies include ZPE and are relative to the lowest energy conformer of neutral methoxymethanol.

Conclusion

In summary, the observed absence of the methoxymethanol parent cation and our calculations imply that dissociative ionization of the parent cation is energetically and kinetically favored. These features of the photoionization of methoxymethanol are shared by those of other oxygenates. For example, the dominance of the H-loss channel and observed absence of the parent cation are also known to be characteristic of the ionization of dimethoxymethane, a structurally similar molecule.[30,41] The lack of parent cation signal of dimethoxymethane ionization has been attributed to rapid ionic dissociation occurring on the order of 10^7 s^{-1}.[41]

This study demonstrates that the prominent $[C_2H_5O_2]^+$ fragment with m/z 61 and its energy threshold for ionization at 10.24 ± 0.05 eV serve as a fingerprint of methoxymethanol. Our analysis shows that isomerization from the lowest energy to the higher energy conformers, via TS_{conf}, is slower than H-loss from the lowest energy conformer, for entropic reasons. However, both the low-energy conformer of the cation and the higher-energy conformer group seem to dissociate to yield an H-atom with rate coefficients that yields fragments at 10.21-10.22 eV, in very good accordance with the current experimental observations. While uncertainties in the tunneling treatment and energy thresholds remain, our results suggest that the early, low-energy part of the m/z 61 experimental signal is at least partially due to significant tunneling contributions.

Supplementary Material

Details of ionization energy determination, additional experimental results, details of geometry and energetics calculations, Figures S1-S5 (experimental ionization energy determinations, experimental photoionization spectra, methoxymethanol conformer ionization energies, and methoxymethanol free energy diagram), Tables S1-S3 (methoxymethanol neutral, cation, H-loss saddle point geometries, frequencies, and energies, and calculated ionization energies of methoxymethanol radicals).

Acknowledgements

C.X.K., N.A.H., L.R.F., S.M.G., W.Z. and T.D.P. acknowledge support from the Gas-Phase Chemical Physics (GPCP) and Catalysis Science programs of the Chemical Sciences, Geosciences, and Biosciences (CSGB) Division of the US Department of Energy (USDOE) Basic Energy Sciences (BES) program under grant DE-SC0020320. This research used resources of the Advanced Light Source, which is a DOE Office of Science User Facility under Contract No. DE-ACO2-05CH11231. J.Z. was supported by the Exascale Catalytic Chemistry (ECC) Project, which is supported by the USDOE, Office of Science, BES, CSGB Division, as part of the Computational Chemistry Sciences Program. D. L. O. and N. H. were supported by the CSGB Division, BES, USDOE. Sandia National Laboratories is a multi-mission laboratory managed and operated by National Technology & Engineering Solutions of Sandia, LLC (NTESS), a wholly owned subsidiary of Honeywell International Inc., for the U.S. Department of Energy's National Nuclear Security Administration (DOE/NNSA) under contract DE-NA0003525. This written work is authored by an employee of NTESS. The employee, not NTESS, owns the right, title and interest in and to the written work and is responsible for its contents. Any subjective views or opinions that might be expressed in the written work do not necessarily represent the

views of the U.S. Government. The publisher acknowledges that the U.S. Government retains a non-exclusive, paid-up, irrevocable, world-wide license to publish or reproduce the published form of this written work or allow others to do so, for U.S. Government purposes. The DOE will provide public access to results of federally sponsored research in accordance with the DOE Public Access Plan. Professor Ambarish Kulkarni is acknowledged for supervision of T.D.P.

Author Declarations

Conflict of Interest – The authors have no conflicts to disclose.

Author Contributions

N. A. H: Performed photoionization experiments and data analysis, manuscript writing, editing, and revising.
T. D. P.: Carried out theoretical calculations and analysis, manuscript writing, editing, and revising.
L. R. F.: Performed photoionization experiments.
S. M. G.: Performed photoionization experiments and catalyst synthesis.
W. Z.: Performed photoionization experiments.
N. H.: Acquired financial support, advised on data collection and formal analysis techniques, and edited/revised the manuscript.
D.L.O.: Acquired financial support, advised on data collection and formal analysis techniques, and edited/revised the manuscript.
J. Z.: Acquired financial support, carried out theoretical calculations and analysis, and edited/revised the manuscript.
C. X. K.: Managed study, supervised N.A.H., L.R.F., W.Z., and S.M.G., acquired financial support, assisted with manuscript writing/editing.

Data Availability Statement

The data that support the findings of this study are available from the corresponding author upon reasonable request.

References

[1] J. Sambeth, L. Gambaro, and H. Thomas, “Study of the Adsorption/Oxidation of Methanol over Vanadium Pentoxide,” Adsorption Science & Technology **12**(3), 171–180 (1995).

[2] J.-M. Tatibouët, and H. Lauron-Pernot, “Transient Isotopic Study of Methanol Oxidation on Unsupported V_2O_5 Mechanism of Methylal Formation,” Journal of Molecular Catalysis A: Chemical **171**, 205–216 (2001).

[3] J.E. Sambeth, M.A. Centeno, A. Paúl, L.E. Briand, H.J. Thomas, and J.A. Odriozola, "In Situ DRIFTS Study of the Adsorption-Oxidation of CH_3OH on V_2O_5," Journal of Molecular Catalysis A: Chemical **161**, 89–97 (2000).

[4] K.K. Barakoti, P. Subedi, F. Chalyavi, S. Gutierrez-Portocarrero, M.J. Tucker, and M.A. Alpuche-Aviles, "Formaldehyde Analysis in Non-Aqueous Methanol Solutions by Infrared Spectroscopy and Electrospray Ionization," Frontiers in Chemistry **9**, 678112 (2021).

[5] D.C. Silverman, and J.J. Freeman, "Associated Species in Vaporized Methanol-Formaldehyde Solutions," Industrial & Engineering Chemistry Process Design and Development **22**, 441–445 (1983).

[6] M. Detcheberry, P. Destrac, X.M. Meyer, and J.S. Condoret, "Phase Equilibria of Aqueous Solutions of Formaldehyde and Methanol: Improved Approach Using UNIQUAC Coupled to Chemical Equilibria," Fluid Phase Equilibria **392**, 84–94 (2015).

[7] C. Kuhnert, M. Albert, S. Breyer, I. Hahnenstein, H. Hasse, and G. Maurer, "Phase Equilibrium in Formaldehyde Containing Multicomponent Mixtures: Experimental Results for Fluid Phase Equilibria of (Formaldehyde + (Water or Methanol) + Methylal) and (Formaldehyde + Water + Methanol + Methylal) and Comparison with Predictions," Industrial & Engineering Chemistry Research **45**(14), 5155–5164 (2006).

[8] S. Dwivedi, S.H. Mushrif, A.L. Chaffee, and A. Tanksale, "Solvation Behaviour and Micro-Phase Structure of Formaldehyde-Methanol-Water Mixtures," Journal of Molecular Liquids **301**, 112444 (2020).

[9] G. Maurer, "Vapor-Liquid Equilibrium of Formaldehyde-and Water-Containing Multicomponent Mixtures," AIChE Journal **32**(6), 932–948 (1986).

[10] A.A. Konnov, E.J.K. Nilsson, M. Christensen, and C.-W. Zhou, "Combustion Chemistry of Methoxymethanol. Part II: Laminar Flames of Methanol+Formaldehyde Fuel Mixtures," Combustion and Flame **229**, 111411 (2021).

[11] S.M. Gurses, T. Price, A. Zhang, J.H. Frank, N. Hansen, D.L. Osborn, A. Kulkarni, and C.X. Kronawitter, "Near-Surface Gas-Phase Methoxymethanol Is Generated by Methanol Oxidation over Pd-Based Catalysts," Journal of Physical Chemistry Letters **12**(46), 11252–11258 (2021).

[12] B. Zhou, E. Huang, R. Almeida, S. Gurses, A. Ungar, J. Zetterberg, A. Kulkarni, C.X. Kronawitter, D.L. Osborn, N. Hansen, and J.H. Frank, "Near-Surface Imaging of the Multicomponent Gas Phase above a Silver Catalyst during Partial Oxidation of Methanol," ACS Catalysis **11**(1), 155–168 (2021).

[13] S.M. Gurses, N. Felvey, L.R. Filardi, A.J. Zhang, J. Wood, K. van Benthem, J.H. Frank, D.L. Osborn, N. Hansen, and C.X. Kronawitter, "Constraining Reaction Pathways for Methanol Oxidation Through Operando Interrogation of Both the Surface and the Near-Surface Gas Phase," Chem Catalysis **3**(10), 100782 (2023).

[14] H. Liu, and E. Iglesia, “Selective One-Step Synthesis of Dimethoxymethane via Methanol or Dimethyl Ether Oxidation on $H_{3+n}V_nMo_{12-n}PO_{40}$ Keggin Structures,” Journal of Physical Chemistry B **107**(39), 10840–10847 (2003).

[15] J. Lichtenberger, D. Lee, and E. Iglesia, “Catalytic Oxidation of Methanol on Pd Metal and Oxide Clusters at Near-Ambient Temperatures,” Physical Chemistry Chemical Physics **9**(35), 4902 (2007).

[16] K. Takahashi, N. Takezawa, and H. Kobayashi, “Mechanism of Formation of Methyl Formate from Formaldehyde over Copper Catalysts,” Chemistry Letters **12**(7), 1061–1064 (1983).

[17] H. Liu, and E. Iglesia, “Selective Oxidation of Methanol and Ethanol on Supported Ruthenium Oxide Clusters at Low Temperatures,” Journal of Physical Chemistry B **109**(6), 2155–2163 (2005).

[18] Y. Zhu, C.-W. Zhou, and A.A. Konnov, “Combustion Chemistry of Methoxymethanol. Part I: Chemical Kinetics of Hydrogen-Abstraction Reactions and the Unimolecular Reactions of the Product [$C_2H_5O_2$] Radicals,” Combustion and Flame **229**, 111396 (2021).

[19] B.A. McGuire, C.N. Shingledecker, E.R. Willis, A.M. Burkhardt, S. El-Abd, R.A. Motiyenko, C.L. Brogan, T.R. Hunter, L. Margulès, J.-C. Guillemin, R.T. Garrod, E. Herbst, and A.J. Remijan, “ALMA Detection of Interstellar Methoxymethanol (CH_3OCH_2OH),” The Astrophysical Journal **851**(2), L46 (2017).

[20] R.A. Johnson, and A.E. Stanley, “GC/MS and FT-IR Spectra of Methoxymethanol,” Applied Spectroscopy **45**(2), 218–222 (1991).

[21] S. Maity, R.I. Kaiser, and B.M. Jones, “Formation of Complex Organic Molecules in Methanol and Methanol-Carbon Monoxide Ices Exposed to Ionizing Radiation - A Combined FTIR and Reflectron Time-of-Flight Mass Spectrometry Study,” Physical Chemistry Chemical Physics **17**(5), 3081–3114 (2015).

[22] C. Zhu, R. Frigge, A. Bergantini, R.C. Fortenberry, and R.I. Kaiser, “Untangling the Formation of Methoxymethanol (CH_3OCH_2OH) and Dimethyl Peroxide (CH_3OOCH_3) in Star-forming Regions,” The Astrophysical Journal **881**(2), 156-165 (2019).

[23] A.M. Turner, A. Bergantini, A.S. Koutsogiannis, N.F. Kleimeier, S.K. Singh, C. Zhu, A.K. Eckhardt, and R.I. Kaiser, “A Photoionization Mass Spectrometry Investigation into Complex Organic Molecules Formed in Interstellar Analog Ices of Carbon Monoxide and Water Exposed to Ionizing Radiation,” The Astrophysical Journal **916**(2), 74-85 (2021).

[24] R.A. Motiyenko, L. Margulès, D. Despois, and J.-C. Guillemin, “Laboratory Spectroscopy of Methoxymethanol in the Millimeter-Wave Range,” Physical Chemistry Chemical Physics **20**(8), 5509–5516 (2018).

[25] T.D. Harris, D.H. Lee, M.Q. Blumberg, and C.R. Arumainayagam, “Electron-Induced Reactions in Methanol Ultrathin Films Studied by Temperature-Programmed Desorption: A Useful Method to Study Radiation Chemistry,” Journal of Physical Chemistry **99**, 9530–9535 (1995).

[26] N. Hansen, T.A. Cool, P.R. Westmoreland, and K. Kohse-Höinghaus, “Recent Contributions of Flame-Sampling Molecular-Beam Mass Spectrometry to a Fundamental Understanding of Combustion Chemistry,” Progress in Energy and Combustion Science **35**(2), 168–191 (2009).

[27] T.A. Cool, K. Nakajima, T.A. Mostefaoui, F. Qi, A. McIlroy, P.R. Westmoreland, M.E. Law, L. Poisson, D.S. Peterka, and M. Ahmed, “Selective Detection of Isomers with Photoionization Mass Spectrometry for Studies of Hydrocarbon Flame Chemistry,” Journal of Chemical Physics **119**(16), 8356–8365 (2003).

[28] K. Moshammer, A.W. Jasper, D.M. Popolan-Vaida, A. Lucassen, P. Diévart, H. Selim, A.J. Eskola, C.A. Taatjes, S.R. Leone, S.M. Sarathy, Y. Ju, P. Dagaut, K. Kohse-Höinghaus, and N. Hansen, “Detection and Identification of the Keto-Hydroperoxide ($HOOCH_2OCHO$) and Other Intermediates during Low-Temperature Oxidation of Dimethyl Ether,” Journal of Physical Chemistry A **119**(28), 7361–7374 (2015).

[29] T.A. Cool, J. Wang, K. Nakajima, C.A. Taatjes, and A. McIlroy, “Photoionization Cross Sections for Reaction Intermediates in Hydrocarbon Combustion,” International Journal of Mass Spectrometry **247**(1–3), 18–27 (2005).

[30] B. Yang, J. Wang, T.A. Cool, N. Hansen, S. Skeen, and D.L. Osborn, “Absolute Photoionization Cross-Sections of Some Combustion Intermediates,” International Journal of Mass Spectrometry **309**, 118–128 (2012).

[31] J. Wang, B. Yang, T.A. Cool, and N. Hansen, “Absolute Cross-Sections for Dissociative Photoionization of Some Small Esters,” International Journal of Mass Spectrometry **292**(1–3), 14–22 (2010).

[32] H.P. Aytam, V. Akula, K. Janmanchi, S.R. Rao Kamaraju, K. Rao Panja, K. Gurram, and J.W. Niemantsverdriet, “Characterization and Reactivity of Pd/MgO and Pd/γ-Al2O3 Catalysts in the Selective Hydrogenolysis of CCl_2F_2,” Journal of Physical Chemistry B **106**(5), 1024–1031 (2002).

[33] R. Van de Vijver, and J. Zádor, “KinBot: Automated Stationary Point Search on Potential Energy Surfaces,” Computer Physics Communications **248**, 106947 (2020).

[34] J. Zádor, C. Martí, R. Van De Vijver, S.L. Johansen, Y. Yang, H.A. Michelsen, and H.N. Najm, “Automated Reaction Kinetics of Gas-Phase Organic Species over Multiwell Potential Energy Surfaces,” Journal of Physical Chemistry A **127**(3), 565–588 (2022).

[35]J. A. Montgomery Jr., M. J. Frisch, J. W. Ochterski, and G. A. Petersson, “A complete basis set model chemistry. VII. Use of the minimum population localization method,” J. Chem. Phys. **112**, 6532–6542 (2000).

[36] M. J. Frisch, G. W. Trucks, H. B. Schlegel, G. E. Scuseria, M. A. Robb, J. R. Cheeseman, G. Scalmani, V. Barone, G. A. Petersson, H. Nakatsuji, X. Li, M. Caricato, A. V. Marenich, J. Bloino, B. G. Janesko, R. Gomperts, B. Mennucci, H. P. Hratchian, J. V. Ortiz, A. F. Izmaylov, J. L. Sonnenberg Williams, F. Ding, F. Lipparini, F. Egidi, J. Goings, B. Peng, A. Petrone, T. Henderson, D. Ranasinghe, V. G. Zakrzewski, J. Gao, N. Rega, G. Zheng, W. Liang, M. Hada, M. Ehara, K. Toyota, R. Fukuda, J. Hasegawa, M. Ishida, T. Nakajima, Y. Honda, O. Kitao, H. Nakai, T. Vreven, K. Throssell, J. A. Montgomery, Jr., J. E. Peralta, F. Ogliaro, M. J. Bearpark, J. J. Heyd, E. N. Brothers, K. N. Kudin, V. N. Staroverov, T. A. Keith, R. Kobayashi, J. Normand, K. Raghavachari, A. P. Rendell, J. C. Burant, S. S. Iyengar, J. Tomasi, M. Cossi, J. M. Millam, M. Klene, C. Adamo, R. Cammi, J. W. Ochterski, R. L. Martin, K. Morokuma, O. Farkas, J. B. Foresman, and D. J. Fox, Gaussian 16, Rev. B. 01, Wallingford, CT, 2016.

[37] H.-J. Werner, P. J. Knowles, G. Knizia, F. R. Manby, M. Schütz, M. Celani, W. Györffy, D. Kats, T. Korona, R. Lindh, A. Mitrushenkov, G. Rauhut, K. R. Shamasundar, T. B. Adler, R. D. Amos, S. J. Bennie, A. Bernhardsson, A. Berning, D. L. Cooper, M. J. O. Deegan, A. J. Dobbyn, F. Eckert, E. Goll, C. Hampel, A. Hesselmann, G. Hetzer, T. Hrenar, G. Jansen, C. Köppl, Y. Liu, A. W. Lloyd, Q. Ma, R. A. Mata, A. J. May, S. J. McNicholas, H. Meyer, T. F. Miller III, M. E. Mura, A. Nicklass, D. P. O'Neill, P. Palmieri, D. Peng, T. Petrenko, K. Pflüger, R. Pitzer, M. Reiher, T. Shiozaki, H. Stoll, A. J. Stone, R. Tarroni, T. Thorsteinsson, M. Wang, and M. Welborn, MOLPRO, version 2022, a package of ab initio programs (2022). http://www.molpro.net

[38] Y. Georgievskii, and S. J. Klippenstein, "Master Equation System Solver (MESS)," https://github.com/Auto-Mech/MESS/ (2016).

[39] K.K. Sullivan, M.D. Boamah, K.E. Shulenberger, S. Chapman, K.E. Atkinson, M.C. Boyer, and C.R. Arumainayagam, "Low-Energy (<20 eV) and High-Energy (1000 eV) Electron-Induced Methanol Radiolysis of Astrochemical Interest," Monthly Notices of the Royal Astronomical Society **460**(1), 664–672 (2016).

[40] G. Meloni, P. Zou, S.J. Klippenstein, M. Ahmed, S.R. Leone, C.A. Taatjes, and D.L. Osborn, "Energy-Resolved Photoionization of Alkylperoxy Radicals and the Stability of their Cations," Journal of the American Chemical Society **128**(41), 13559–13567 (2006).

[41] T. Yu, X. Wu, X. Zhou, A. Bodi, and P. Hemberger, "Hydrogen Migration as a Potential Driving Force in the Thermal Decomposition of Dimethoxymethane: New Insights from Pyrolysis Imaging Photoelectron Photoion Coincidence Spectroscopy and Computations," Combustion and Flame **222**, 123–132 (2020).

[42] B.M. Hays, and S.L. Widicus Weaver, "Theoretical Examination of O(^{1}D) Insertion Reactions to Form Methanediol, Methoxymethanol, and Aminomethanol," Journal of Physical Chemistry A **117**(32), 7142–7148 (2013).

[43] M. Kamphus, N.-N. Liu, B. Atakan, F. Qi, and A. McIlroy, "REMPI temperature measurement in molecular beam sampled low-pressure flames," Proceedings of the Combustion Institute **29**(2), 2627–2633 (2002).